Defence Research and   Recherche et développement
Development Canada   pour la défense Canada

DEFENCE **R&D** DÉFENSE

Numerical and experimental investigations of transformations of near-field to far-field scattering measurements

John A. Fawcett
J. Sildam
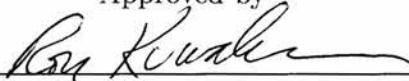*M. Trevorrow*

Defence R&D Canada – Atlantic

Technical Memorandum
DRDC Atlantic TM 2006-082
July 2006

Canada

This page intentionally left blank.

Numerical and experimental investigations of transformations of near-field to far-field scattering measurements

John A. Fawcett

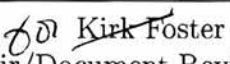J. Sildam

M. Trevorrow

Author

John Fawcett

Approved by

Ron Kuwahara
Head/Signatures

Approved for release by

Dr. Kirk Foster
Chair/Document Review Panel

Abstract

Measurements of monostatic target strength are often made in the near field of the target. This memorandum investigates some model-based inversion techniques which can be used to predict far-field monostatic target strengths as a function of aspect angle from the near field measurements. Simulated and experimental data are used to illustrate the accuracy of the proposed methods.

Résumé

Les mesures d'intensité de cible monostatique sont souvent prises en champ proche. Le présent document examine des techniques d'inversion basées sur des modèles, qui peuvent servir à prévoir l'intensité de cible monostatique en champ lointain selon l'angle d'aspect obtenu en champ proche. Des données de simulations et d'expériences montrent l'exactitude des méthodes proposées.

This page intentionally left blank.

Executive summary

Numerical and experimental investigations of transformations of near-field to far-field scattering measurements

John A. Fawcett, J. Sildam, M. Trevorrow; DRDC Atlantic TM 2006-082; Defence R&D Canada – Atlantic; July 2006.

Background

The measurement and knowledge of target scattering strength is important for many sonar applications. However, in many cases because of a target's size and the limited size of the measurement facility, it is not possible to make the scattering measurements in the far field of the target. In this report, possible methods for predicting target strength (as a function of aspect) from near field scattering measurements are investigated.

Principal results

It was found that basic Kirchhoff modeling of a target gave reasonably accurate estimates of the broadside and endcap target strengths. However, for the experimental target considered, it failed to capture much of the detailed structure of the target strength as a function of aspect angle. In general, the methods, based upon first determining model coefficients from near field measurements, predicted the farther range measurements with more accuracy.

Significance of results

In situations where the direct measurement of far field target scattering strengths is not possible, the methods of this report could provide a means of predicting the far field scattering strengths based on near field measurements.

Future work

The use of the methods of this paper with more experimental data sets would be useful in establishing the applicability of the methods. Combining the inversion methods with apriori knowledge of the target strengths in some directions would also be an interesting area of research. Also, the use of data for 2 different ranges might be used to improve the robustness and accuracy of the method.

This page intentionally left blank.

Sommaire

Numerical and experimental investigations of transformations of near-field to far-field scattering measurements

John A. Fawcett, J. Sildam, M. Trevorrow; DRDC Atlantic TM 2006-082; R & D pour la défense Canada – Atlantique; July 2006.

Introduction

La mesure et la connaissance de l'intensité de diffusion de cibles sont importantes pour de nombreuses applications sonar. Toutefois, la taille de la cible et les dimensions limitées de l'installation de mesure ne permettent souvent pas de mesurer la diffusion en champ lointain. Le présent rapport examine des méthodes possibles pour prévoir l'intensité de cible (selon l'aspect) à partir de mesures de diffusion en champ proche.

Résultats

On a constaté que la modélisation de base de Kirchhoff d'une cible estime de manière raisonnablement exacte les intensités de rayonnement transversal et longitudinal des cibles. Toutefois, pour la cible expérimentale considérée, l'angle d'aspect a peu révélé la structure détaillée de l'intensité de la cible. Les méthodes, basées sur la détermination initiale de coefficients de modèles à partir de mesures en champ proche, ont en général produit des prévisions plus exactes des mesures au lointain.

Portée

Lorsque les intensités de diffusion en champ lointain ne sont pas directement mesurables, les méthodes présentées ici pourraient permettre de prévoir les intensités de diffusion en champ lointain à partir des mesures en champ proche.

Recherches Futures

L'utilisation de plus larges ensembles de données expérimentales avec les méthodes présentées ici serait utile pour établir l'applicabilité de celles-ci. Il serait également intéressant d'étudier la combinaison des méthodes d'inversion avec une connaissance a priori des intensités des cibles dans certaines directions. En outre, l'utilisation de données pour deux distances différentes pourrait permettre d'améliorer la robustesse et la précision de la méthode.

This page intentionally left blank.

Table of contents

List of figures

Acknowledgements

We would like to thank Mark Rowsome for his help in setting up the experiments. We are grateful for the helpful comments of David Chapman on an earlier draft version of this report.

This page intentionally left blank.

1 INTRODUCTION

For many sonar applications, the measurement of target scattering strength is important. It is well-known that near-field corrections must be applied for transducer beam-pattern measurements, but corrections also need to be applied to backscatter from elongated targets. This generally arises in a naval context, such as the measurement of backscatter from torpedos [1], ships and submarines. In such cases true far-field measurements are difficult or impossible to make due to the large ranges involved (potentially, greater than hundreds of meters). In some situations, it is possible to get sufficiently far from the target but one then faces acoustic multipath issues in the received signal.

The term "far field" implies that the projector and the receiver are sufficiently far away from the target that the amplitude of the field scattered from the target, for a fixed aspect, depends linearly upon the ranges of the projector and receiver. The near-field problem arises at short ranges where the assumption of acoustic plane-wave behavior breaks down, both for the incident and backscattered fields. In the near-field, the strong directional backscatter peaks are reduced and side-lobe structures are incompletely formed relative to the far-field expectations. Usually what is wanted is the far-field target scattering, as typical detection problems involve distances of order hundreds of meters to kilometers. Simple rules of thumb for far-field distances can be used by assuming the target is similar to an acoustic projector, where there are well-known far-field scales. Hence, for a line-array of length L with acoustic wavelength λ (e.g. modeling the broadside aspect of a cylinder) this far-field scale is $L^2/(2\lambda)$, and for a circular disc of radius a the far-field scale is $\pi^2 a/\lambda$ [2]. Clearly this near-field problem becomes increasingly significant for larger targets, scaling as the square of the diameter and/or length. When the projector and/or receiver are not in the far field of the target, second order effects, such as the curvature of the incident and scattered wavefronts are significant. In [3] Chapman considers a correction of near field measurements by using a Fresnel Integral to account for the phase variations of the field scattered by a target. For the case of measurements using a single source and a set of receivers on a spherical surface which encloses the target of interest, it is straightforward to extrapolate these measurements (with a sufficiently fine spatial sampling) to another range [4]. Varying the source position around the same sphere, one can then extrapolate the entire set of scattering measurements, both mono- and bistatic, to the other range.

The case we consider in this report involves a much simpler measurement geometry. In particular, we consider an axisymmetric or near-axisymmetric target. The measurements will consist of a set of monostatic measurements in a single horizontal plane. This is the geometry which is often used at the DRDC Atlantic measurement facilities, where a single source/hydrophone pair is deployed at a fixed location and

the target is rotated in a horizontal plane. Our basic approach will be to hypothesize some underlying scattering model for the target with a set of unknown coefficients. A set of measurements at one range will be used to determine these coefficients. Once these coefficients are determined they can then be used to predict the scattered field at other ranges (and possibly other angles and waveguide conditions).

The basic concept behind our model-based inversion is that the incident field gives rise to secondary point sources at the target. We will make the hypothesis that the surface field at the point is linearly related to the incident field value by an unknown complex coefficient. In its simplest form we will simply represent the target as a linear array of such sources. In a more complicated approach, we will consider the true shape of a target and consider it as consisting of rings of point sources at specified discrete points. The value of the point source along the ring will be related to its incident value at that location by an unknown coefficient which varies with respect to the ring index. This approach is basically a generalization of the Kirchhoff model of scattering where the coefficients for the "illuminated" portion of the target would be equal to two, and we will refer to this method as a modified Kirchhoff method.

There are related problems in the acoustical, geophysical, medical, and radar communities. One can attempt to reconstruct the actual field values on the surface of the object from its radiated energy. This is the nearfield acoutic holography problem [5,6] and a method which is closely related to ours is the one discussed by Borgiotti and Rosen [7] where they invert near field measurements of an acoustic radiator to determine an equivalent set of point sources. However, it is important to distinguish between the acoustic radiation and acoustic scattering problems. In the latter, we need to hypothesize some simple relation between the incident fields (from our varying projector positions) and the resultant fields upon the target.

Other authors have considered determining the reflectivity of an object or a region from a set of scattering measurements [8,9]. Once the reflectivity is known these values could be used to predict the scattered fields at different locations. One major difference of these types of techniques with our proposed approach is that these methods require a sufficient frequency bandwidth in the signal (and also assume that the reflectivity is constant over the band). Our methods will work with individual frequencies.

This report will present a theoretical overview of the forward and inverse scattering problem, followed by a discussion of results from numerical experiments using well-known full-field acoustic models for objects such as cylinders. These models are able to predict near- and far-field intensities, allowing investigation of near-to-far field transition zones, establishment of rules-of-thumb, and show validity of approximate techniques. Finally, some simple laboratory measurements on a cylindrical target will show the validity of these approximations.

2 THEORY

A simple numerical example can be used to motivate understanding of the near-field problem. Consider the backscatter from a rigid, elongated object to be similar to the reflection from a line-array of N perfectly reflecting point sources with length L, as shown in Fig. 1. In this simple example the source and receiver are located along the perpendicular to the target array, which corresponds acoustically to a broad-side maximum (a glint) from an elongated object. In principle the source and receiver can be at different distances, d_S and d_R, respectively. The source emits a continuous sinusoidal signal with amplitude A, frequency f, and wavenumber k. Spherical spreading is assumed. With these assumptions, the backscattered pressure P_j from the j'th target element at the receiver location can be given by

$$P_j = \frac{A}{r_{Sj}r_{Rj}} \exp(ikr_{Sj}) \exp(ikr_{Rj}) \tag{1}$$

where r_{Sj} and r_{Rj} are the slant ranges from the source and receiver to the k'th element, respectively, and i $= \sqrt{-1}$. Then the total backscattered pressure, P, is just the complex sum over all target elements. This total pressure can then be normalized by our expectation for spherical spreading by multiplying by the source and receiver distances (d_S and d_R) and dividing by the number of target elements. This normalized pressure amplitude is then equivalent to a near-field attenuation, or loss if expressed in decibels.

Let us consider scattering at 10 kHz acoustic frequency, such that the wavelength in water is 0.15 m, from a target array of length 2.0 m composed of 100 elements. The total normalized pressure amplitude vs. range, assuming co-located source and receiver, are then shown in Fig. 2. In this example, the far-field scale is 13.3 m. The figure shows a steady decrease in normalized pressure as the source and receiver location moves closer to the object. At the far-field scale distance the near-field reduction is approximately 3 dB, whereas within one array length of the target the reduction is greater than 14 dB. Physically what is happening here is that in the near-field the difference between the perpendicular distance and slant range becomes a significant fraction of a wavelength, creating an incomplete complex amplitude summation for scattering elements away from the centerline. This is equivalent to a breakdown in the assumption of incident and scattered plane waves that is often made in target scattering problems. This example demonstrates that even for relatively modest sized objects (on naval scales), the necessary far-field distances can easily reach into the 10's of meters.

In the following analysis, we will consider the scattering from a target to be represented by a set of point sources. However, the relationship between the incident field and the coefficients for these point sources will be determined by utilizing a set of scattering measurements.
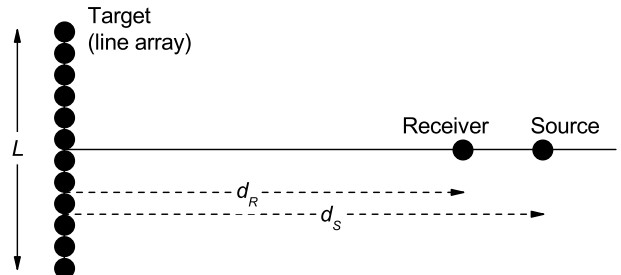
Figure 1: *Schematic diagram of a simple scattering geometry*
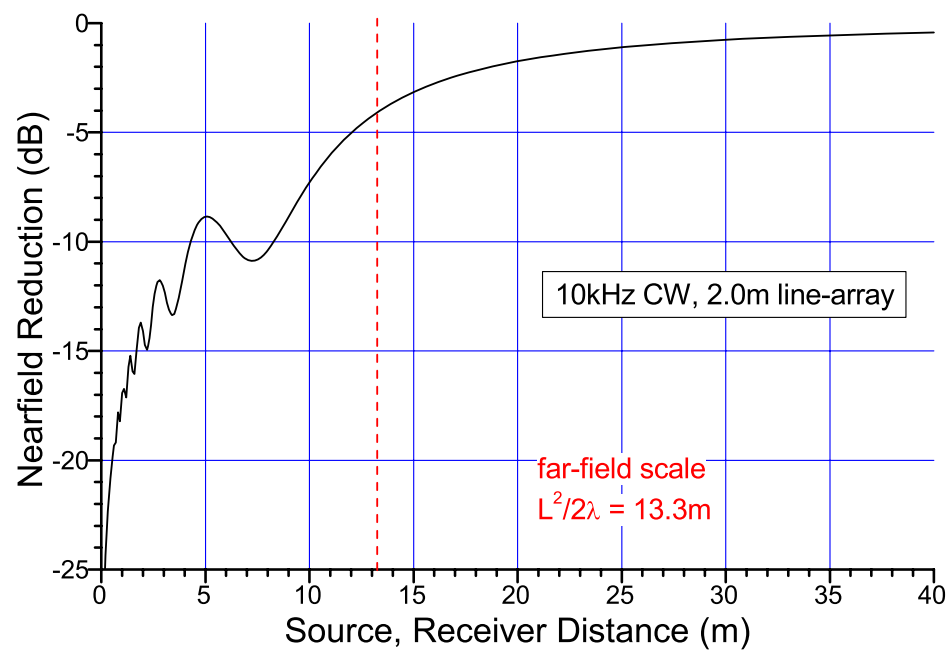
Figure 2: *Normalized total pressure amplitude vs. distance for 10 kHz scattering from a 2.0 m line-array. Source and receiver are co-located.*

For a rigid target, the scattered field anywhere in the surrounding space can be related to the value of the total pressure field upon the surface of the target by the Helmholtz integral[2].

$$p_{sc}(\vec{X}) = -\int_S \frac{\partial G(\vec{X}; \vec{X}(s))}{\partial n} p(\vec{X}(s)) ds \qquad (2)$$

where $\vec{X}$ is a general positional vector, $\vec{X}(s)$ denotes a point on the target surface and G is the Green's Function for the surrounding space. The integral in Eq.(2) is the rigid form of the more general Helmholtz integral [2] which also involves the product of G and $\partial p/\partial n$ on the target surface.

In the Kirchhoff model for rigid target scattering the field upon the target at $\vec{X}(s)$ is simply related to the value of the incident field upon the target,

$$p(\vec{X}(s)) = 2p^{inc}(\vec{X}(s); \vec{X}_0). \qquad (3)$$

Here we have used $\vec{X}_0$ to denote a possible point source location for the incident field. In this case, the incident field has the form

$$p^{inc}(\vec{X}(S); \vec{X}_0) = -\frac{\exp(i2\pi f|\vec{X}(s) - \vec{X}_0|/c)}{4\pi|\vec{X}(s) - \vec{X}_0|}. \qquad (4)$$

The Green's Function which is used in the integral of Eq.(2) has the same form as this point source incident field.

In the Kirchhoff approximation, instead of simply using the value $2p^{inc}$ everywhere on the surface of the target, the pressure values are set to zero at those points on the target surface where they are not illuminated by the source. For example, values on the backside of a cylinder with respect to the insonification direction are set to zero. In some of our examples, the source and receiver will be at different ranges. We will also set pressure value contributions to zero if the normal from the target surface is more than 90° from the ray connecting the point on the surface to the receiver location. For complicated target shapes, one portion of the target could shadow another portion of the target and these regions would need to be determined by ray tracing. In our work we will simply set the pressure values to zero if the normal to the surface is more than 90° with respect to either the incident or target/receiver ray.

For much of the following work we will utilize a cylindrical coordinate system. We consider the surface integral of Eq.(2) in a discrete form with a set of points in the (r, z)) plane (r denotes radius for a cylindrical targets and z is the length along the axis. The variable θ denotes the angular variable around the z-axis. For example, in Fig. 3 we show two of the discretizations we will use for the experimental target. The actual target shapes result from rotating these discretizations around the z-axis. For each of these points and along the circle in r, θ which this point generates,
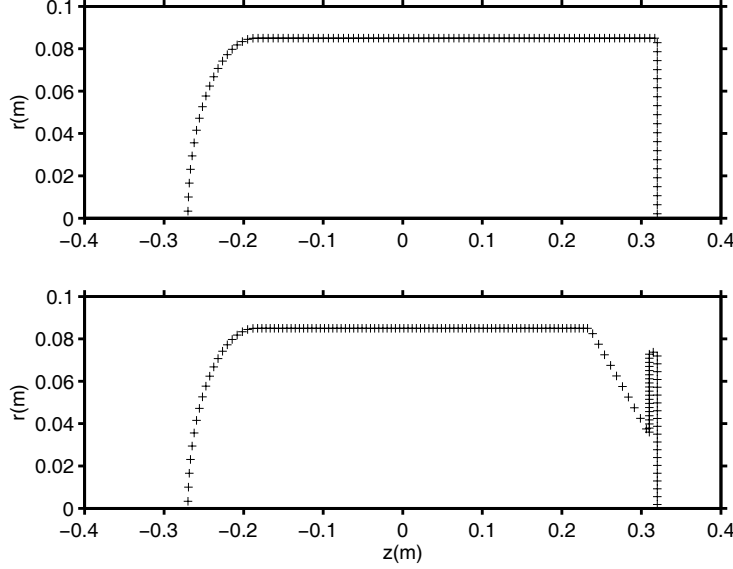
Figure 3: *The 2 discrete targets models for the inverse Kirchhoff method: (top) simplified model (bottom) more accurate model. The vertical axis is radius. The three-dimensional target shape is produced by rotation about the z-axis.*

we suppose that the pressure value is related to the incident pressure value by an unknown coefficient,

$$p(r_i, z_i, \theta) = a_i p^{inc}(r_i, z_i, \theta). \tag{5}$$

The constant of proportionality a_i depends only upon the (r, z) location of the discrete point but not on θ. For each discrete point (r_i, z_i, θ), the contribution will be set to zero based upon the computed surface normal with respect to the source/target and target/receiver rays. Using the fact that we relate the surface pressure field to the incident field values by a set of unknown complex coefficients (a_k) we finally arrive at the relationship that the pressure field at receivers $\vec{X}_r(j)$ can be written in the form,

$$p(\vec{X}_r(j)) = \sum_{k=1}^{N} S_{jk} a_k, \quad j = 1, ..., M \tag{6}$$

where the elements of the matrix S_{jk} are given by

$$S_{jk} = r_k \Delta_k \int_0^{2\pi} w_k(\theta) \frac{\partial}{\partial n_s} G(\vec{X}_r(j); \vec{X}(r_k, z_k, \theta)) G(\vec{X}(r_k, z_k, \theta); \vec{X}_0(j)) d\theta. \tag{7}$$

In this equation, the normal derivative is with respect to the surface variables and $w_k(\theta)$ is zero when the ray from the source or to the receiver makes an angle of greater than $90°$ with the surface normal vector. The variable r_k is the cylindrical radius and Δ_k is the length of the discrete surface element. The term $\vec{X}_0(j)$ denotes the

point source location for the jth measurement. The integrals in Eq.(7) are evaluated numerically. From Eq.(6), it can be seen that for M monostatic scattering measurements and N discrete (r, z) points with the corresponding coefficient a_k, we have a system of M equations with N unknowns. We will take $M > N$ and our solution will be the least-squares solution for the coefficients a_k. In the numerical examples which are presented in section 3, the inversion of the matrix S is performed using the MATLAB standard pseudoinverse routine. This function allows one to specify a singular value tolerance. Singular values, whose values are less than the tolerance are set to zero. Once the coefficients a_k are determined, they can then be used again with Eq.(6) with a recomputed version of S_{jk} to predict the scattered fields for a different set of source and receiver positions. If, instead of solving the system of equations for a_k, we simply set them equal to 2 we obtain the Kirchhoff model predictions for the scattered field. The experimental target we will consider is not perfectly rigid so, in fact, there are both p and $\partial p / \partial n$ contributions in the general Helmholtz integral. However, in this report we only attempt to model the "effective" values of p on the surface and will use the form of the Helmholtz equation given by Eq.(2).

A simplification occurs if we let the radius of the object shrink to zero. In this case we have a line array of point sources with specified positions $(z_k, k = 1, ..., N)$. Furthermore, we do not use the normal derivative and all sources are taken to be illuminated. In this case, we are inverting the observations to obtain the complex-coefficients for a line array of point sources. Now, S_{jk} in Eq.(6) has the form,

$$S_{jk} = \frac{\exp(i2\pi f |\vec{X}_r(j) - \vec{X}_k|/c)}{4\pi |\vec{X}_r(j) - \vec{X}_k|} \frac{\exp(i2\pi f |\vec{X}_0(j) - \vec{X}_k|/c)}{4\pi |\vec{X}_0(j) - \vec{X}_k|}, \qquad (8)$$

relating the unknown point source coefficients to the observations.

3 EXAMPLES

3.1 Numerical Simulation

We will start by considering a simulated data example using a cylindrical target proposed for the NATO Undersea research Centre (NURC) workshop on mine scattering modeling. It is a rigid cylinder of length 2.0 m and radius 0.25 m. One endcap is flat and the other is hemispherical. For the length of 2 m, the approximate far-field scale, $L^2/(2\lambda)$, is 6.7 m for 5 kHz. In Fig. 4 the frequency/azimuth response of the target is shown for ranges (both for the point source and the receiver) of 3 and 20 m. The broadside response of the target is much more diffuse and lower in amplitude at the shorter range than at 20 m. This is also evident in the time domain, Fig. 5, where we have used a Gaussian pulse centred at 5 kHz and a standard deviation of 3 kHz in the computations. The time/azimuth response is much more focussed close to broadside for the 20 m range. in addition, some of the diffraction events (the 2 or 3 lines of arrivals which are evident away from the broadside and endon aspects and which are due to scattering from edges) are relatively stronger. These benchmark results were computed using a boundary-element method [10] for three-dimensional, axially-symmetric targets.

We will consider 3 frequency values from the set of multifrequency data, 1 kHz, 3 kHz, and 9 kHz. First we consider how well the standard Kirchhoff theory does in modelling the responses for these frequencies and for the ranges of 3 and 20 m. For the discrete model of the cylinder, we use 10 discrete points to represent the hemispherical endcap, 10 points to represent the flat endcap and 81 points for the length of the cylinder and then 91 points in azimuth are used for each of these discrete (r, z) points. For a forward prediction using the Kirchhoff method, the coefficients for each of the discrete points which are illuminated is set to 2 and then Eq.s(6) and (7) are used to compute the field at the specified receiver positions. As can be seen in Fig. 6, the predictions (red) are in good agreement with the benchmark solutions, particularly for the highest frequency, 9kHz.

In Fig. 7, we show the results obtained when we first use the near field to invert Eq.(6) for the coefficients to use in the Kirchhoff-like method. The singular values of the matrix were restricted to those with amplitude greater than 2×10^{-5}. The first column of the figure shows the fits of the predicted scattered field curves (red) to the data. The agreement of the curves is expected to be good in this case as this is the data used in the inversion. However, the agreement with the far field results of the second column has noticeably improved. It is interesting to consider the solutions for the coefficients. For our implementation of the Kirchhoff approximation, the values should be -2. In Fig. 8 the real (blue) and imaginary (red) parts of the inverted coefficients are shown for the 3 kHz case. As can be seen, the real parts are quite close to -2, except at the endcaps, particularly for the last coefficients which represent
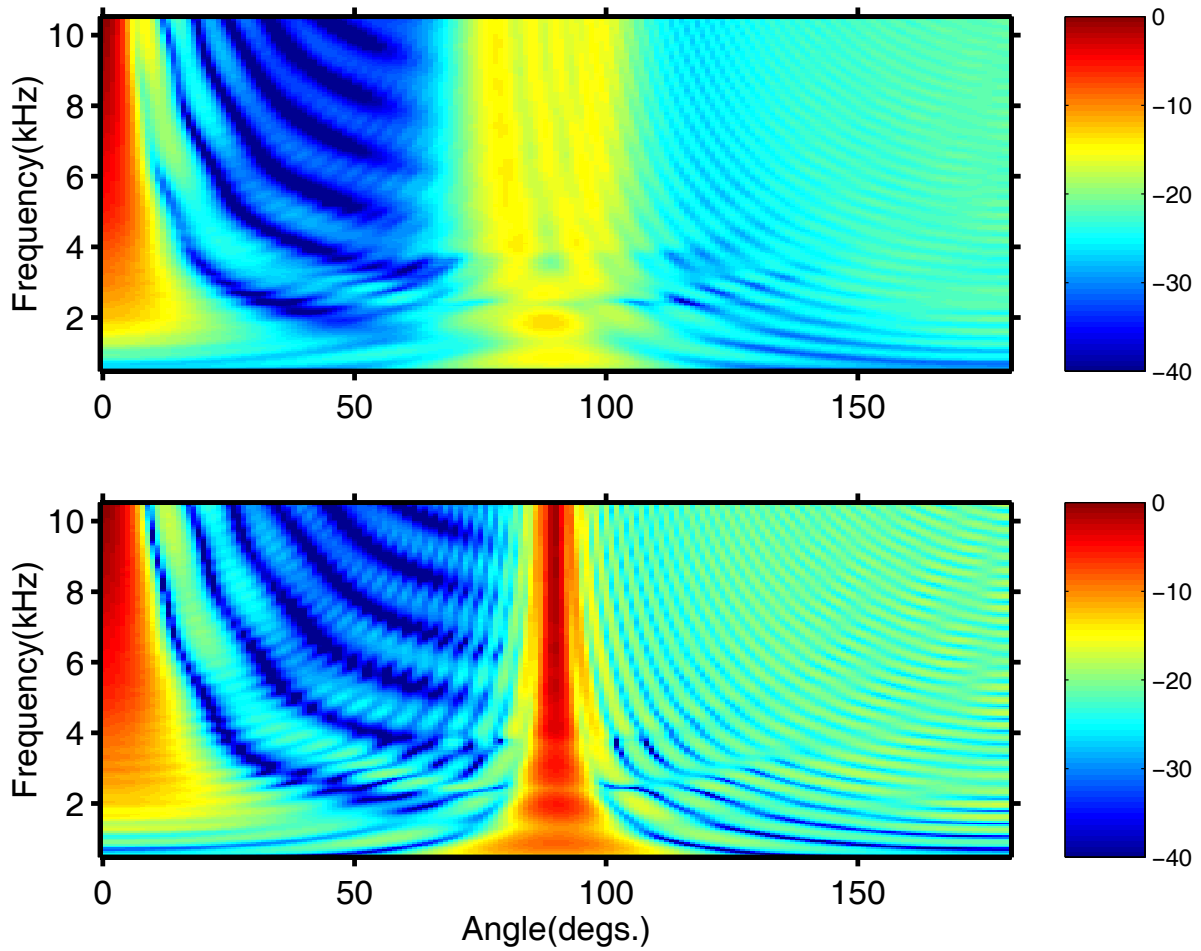
Figure 4: *The frequency/azimuth response (monostatic scattering) of the NURC cylinder for ranges of 3 (upper panel) and 20 m (lower panel). Both plots have been normalized by their maximum absolute values. The flat endcap is the angle 0°, broadside is at 90° and the hemispherical endcap at 180°.*
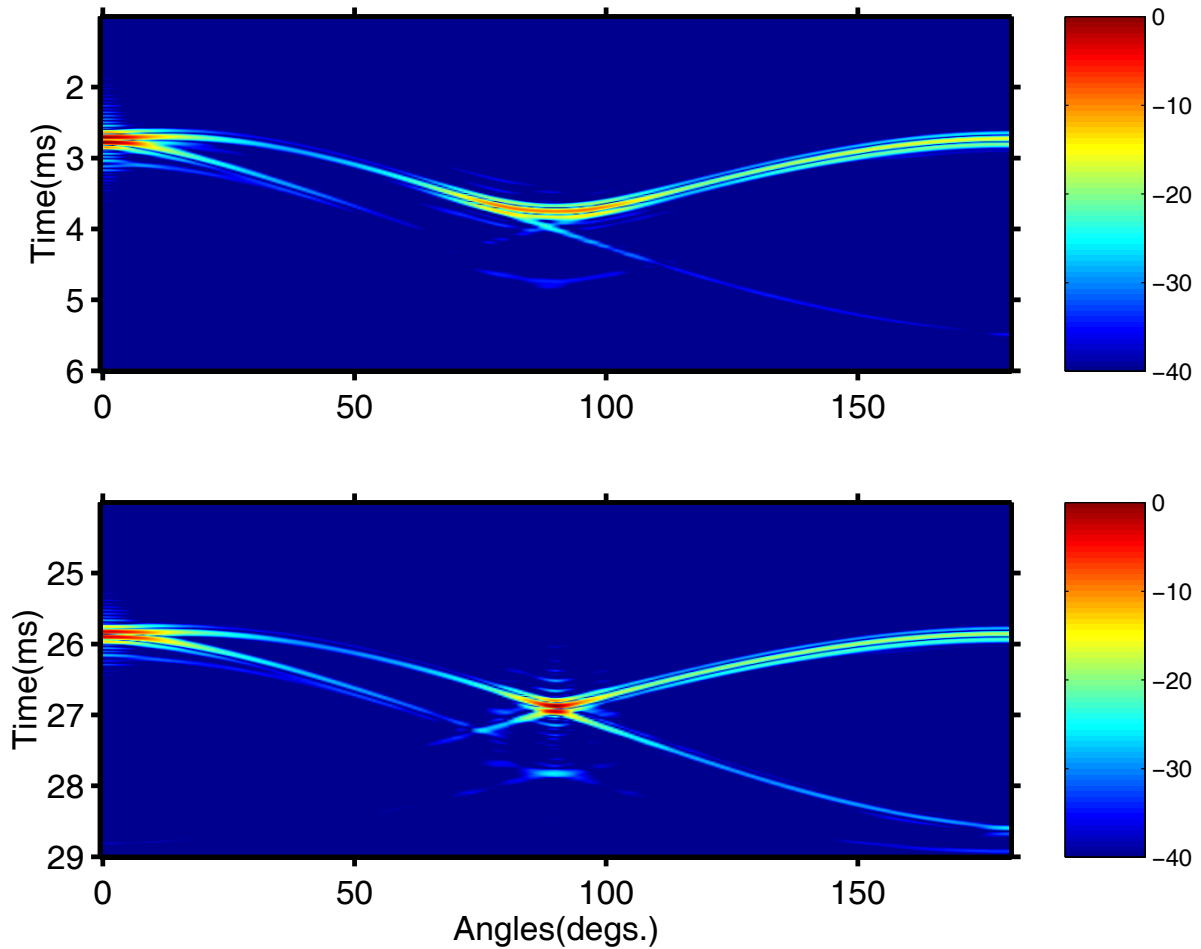
Figure 5: *The times/azimuth response (monostatic scattering) of the NURC cylinder for ranges of 3 (upper) and 20 m (lower). Both plots have been normalized by their maximum absolute values. The flat endcap is the angle 0°, broadside is at 90° and the hemispherical endcap at 180°.*
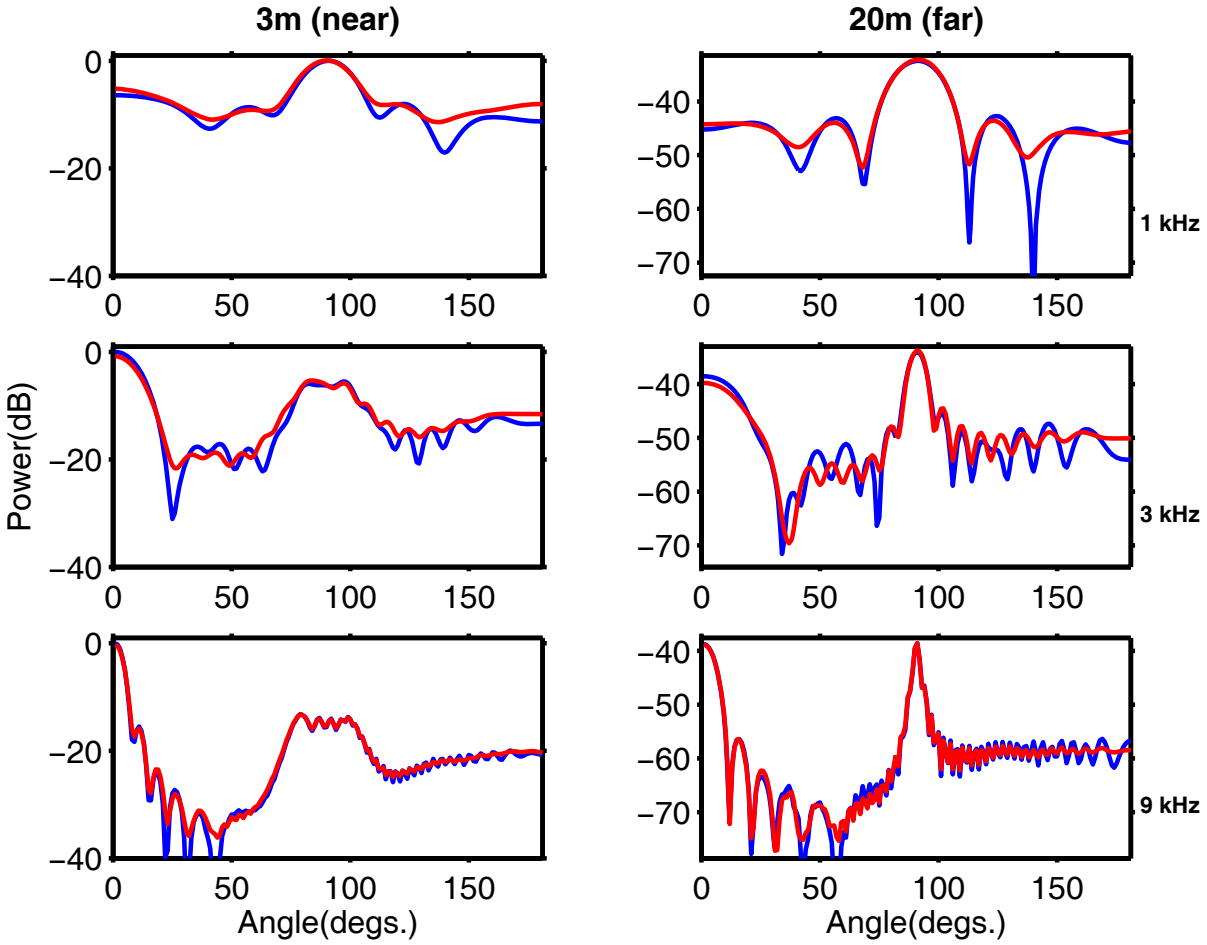
Figure 6: *The benchmark scattered fields as a function of aspect angle (blue) and the Kirchhoff predicted values (red) for column 1, 3 m at 1,3, and 9 kHz and column 2 at 20 m. The curves have been normalized by the maximum amplitude of the benchmark curve*

the flat endcap. The imaginary values are approximately equal to 0.5 instead of the Kirchhoff values of 0.0. Finally we consider a linear array of $N = 121$ sources in the interval $[-1 \quad 1]$ and the nearfield measurements were inverted to determine the coefficients. The singular values were constrained to be greater than 2×10^{-3}. As can be seen in Fig. 9, even with this simple linear array model, the predictions are very good. This is particularly surprising for angles corresponding to the end-caps.

3.2 Experimental Results

The previous example used simulated data where all the parameters were precisely known. It was shown that the 2 prediction methods considered yielded excellent agree-
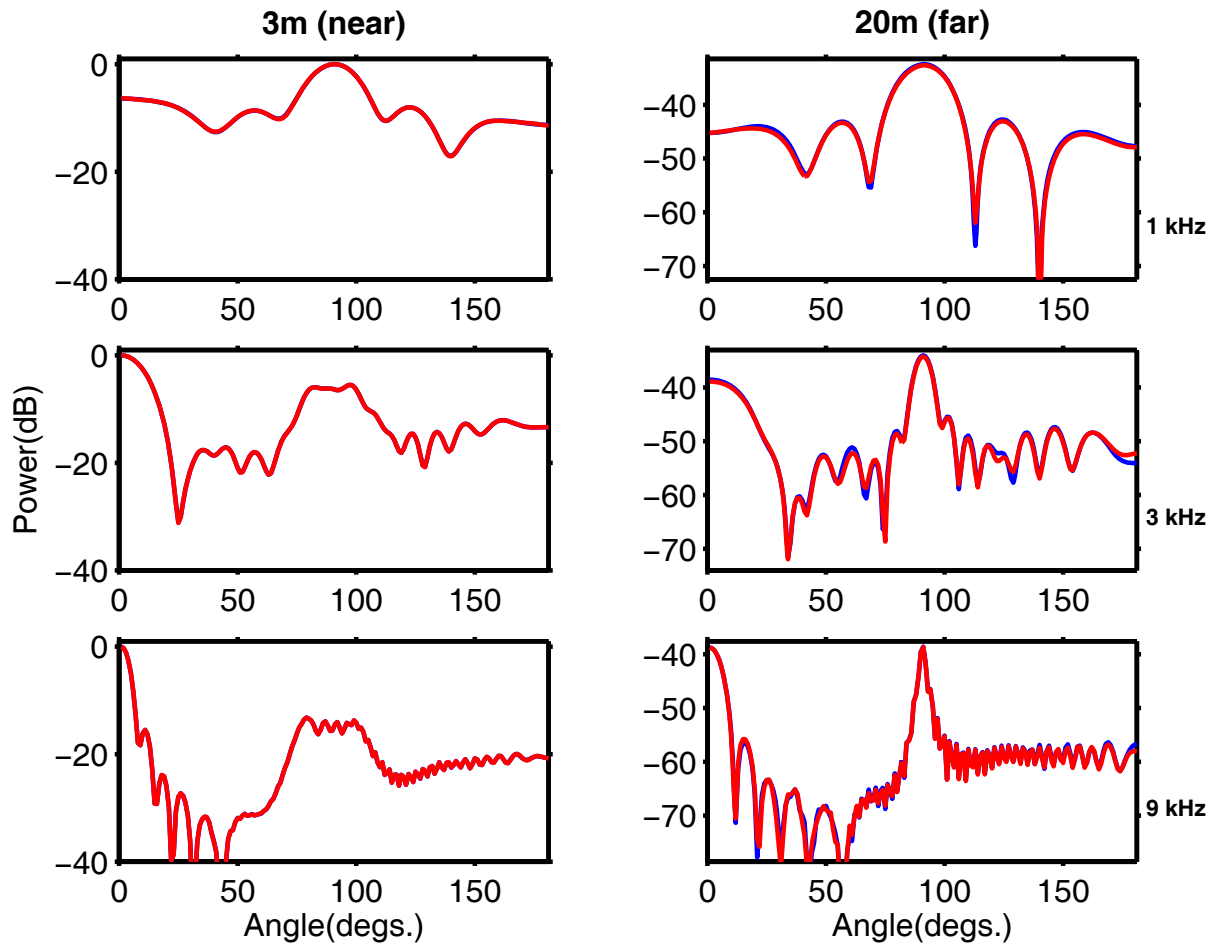
Figure 7: *The benchmark scattered fields as a function of aspect angle (blue) and the Kirchhoff predicted values using the determined coefficients(red) for column 1, 3 m at 1,3, and 9 kHz (these are the fit values) and column 2 at 20 m. The curves have been normalized by the maximum amplitude of the benchmark curve at 3 m range.*
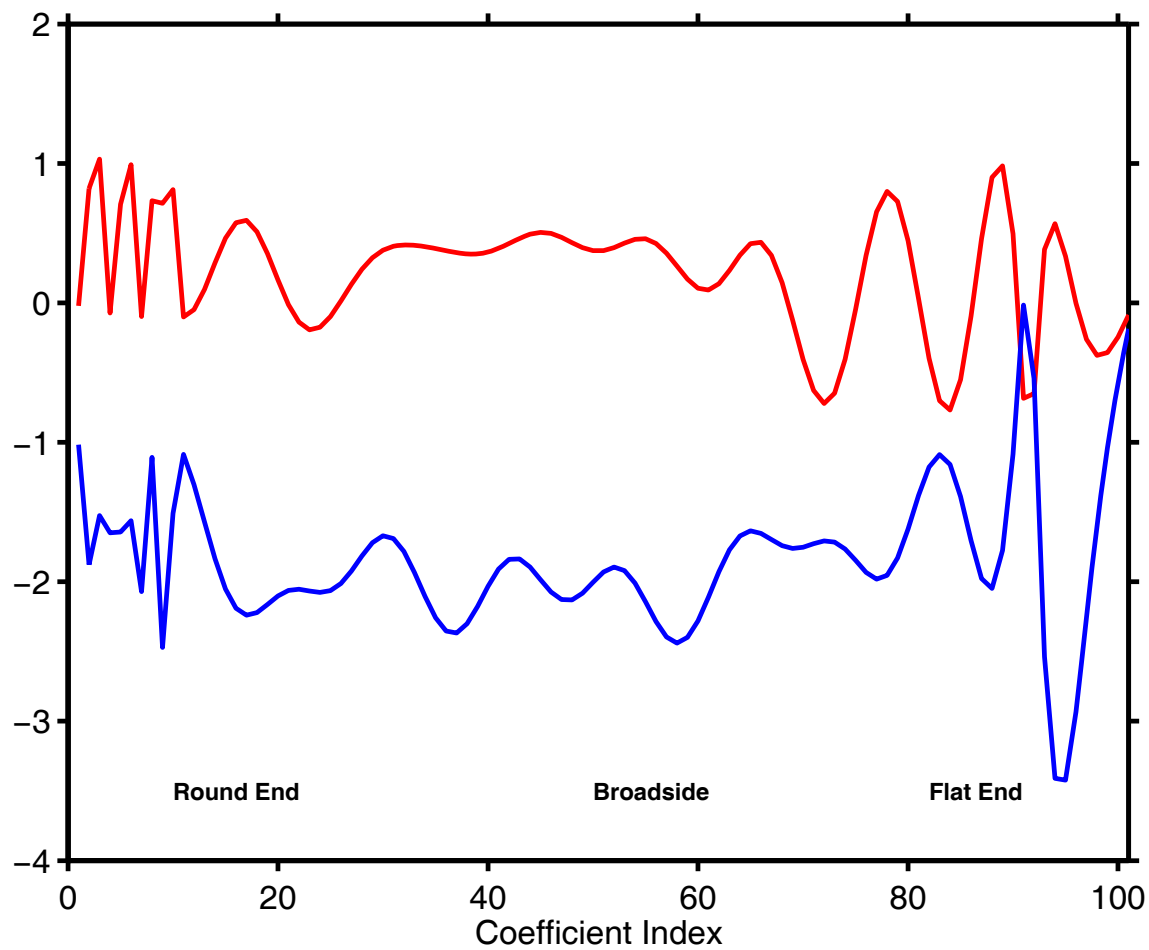
Figure 8: *The determined coefficients for the modified Kirchhoff method at 3 kHz and 3 m. The real part is shown in blue and the imaginary part in red.*
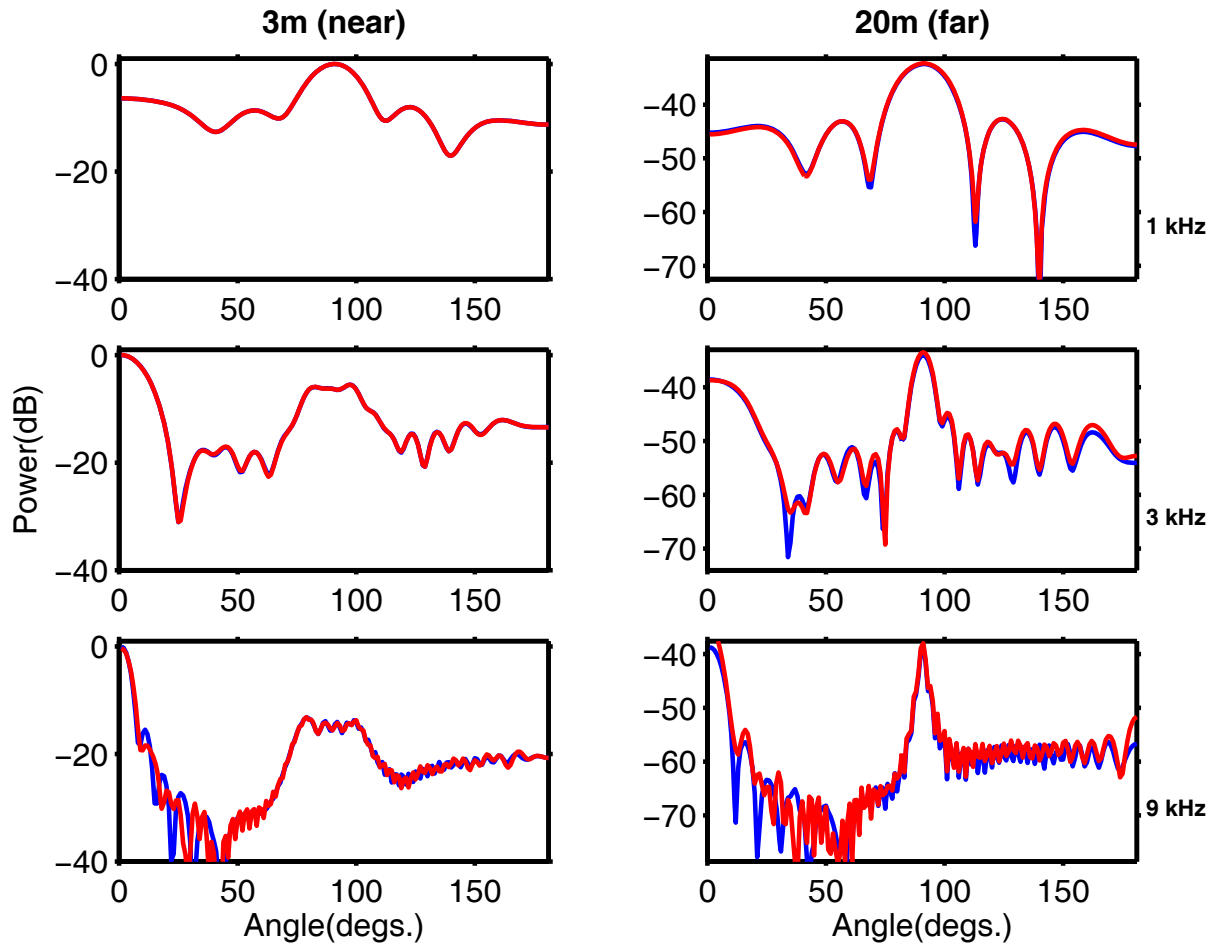
Figure 9: *The benchmark scattered fields as a function of aspect angle (blue) and for the 121-element line array predicted values using the inversion coefficients(red) for column 1, 3 m at 1,3, and 9 kHz (these are the fit values) and column 2 at 20 m. The curves have been normalized by the maximum amplitude of the benchmark curve at 3 m range.*

Figure 10: *The target used in the experiments at DRDC Atlantic acoustic calibration tank*

ment with the benchmark solution. However, simply using the Kirchhoff method, Eqs.(6) and (7) with no inversion modifications, also provided good predictions. However, for practical target scattering measurements, there are a variety of experimental uncertainties. Also, the target scattering will consist of rigid-like components with some elastic effects. Thus, the underlying Kirchhoff model will not be as accurate as for the previously considered simulated example. We now consider some measurements made in the DRDC-Atlantic tank. The target was an old pressure container (see Fig. 10) which was hollow inside (excepting the additional lead weights we added) and was constructed with a rather thick (approx. 1 cm) aluminum casing. It had one hemispherical endcap and also a tapered section ending with a circular flat endcap.

The target was mounted on a rotator at a depth of 2.57 m. The projector, an ITC 1001, and the hydrophone, a Reson 4032, were suspended from another station at the same depth. A sequence of backscatter measurements were made at frequencies

15,20,25,30,35,and 40 kHz. Two different projector/receiver to target distances are considered. There were a number of experimental issues which arose. First, there was only a fairly small interval of ranges where the reflections from the target were isolated from the tail of the incident pulse (because, recall that the amplitude of the incident pulse is significantly higher than the backscattered energy) and the onset of multipath arrivals. For the different frequencies considered, the number of cycles in the harmonic waveform were controlled to try to minimize the interference with the incident pulse. Second, the target was rotated continuously through a nominal interval of 380°. However, the speed of this rotation varied somewhat from one measurement sequence to the next and hence the recorded number of files (pings) for each set were different. In order to compare the near and far measurements and predictions properly, a $\Delta\theta$ was computed for each measurement set by dividing 380° by the number of files. This spacing was then used to align the predicted and measured curves appropriately. The first set of projector/receiver distances from the target were 1.25 m and 0.715 m respectively and these constitute our "near field" measurements. For the further measurements, the distances were 1.72 m and 1.22 m respectively. These distances are still not in the true far field of the target for the broadside aspect, but they do provide a test of being able to accurately translate scattering measurements from one range to those at another. It should be noted that the distances are to the centre of the rotator pole, whereas the distances to points on the target vary. For example, the distance from the projector/receiver to the target endcap is significantly less than the distance to the centre of the cylindrical portion.

In Fig. 11 we show the extracted time series for the scattered field as a function of azimuthal angle at 40 kHz, for the near and far measurements. In this case, and all that follow, the azimuthal angle is 0° at the rounded endcap, 90° and 270° correspond to broadside and 180° to the flat endcap. As can be seen, there may be some interference with the signal and the incident signal for the first few data points for the near field and some interference with multipath arrivals for the last few points for the far range. It can also be seen that the backscattered signal from the endcap arrives a little earlier than the backscattered signal from the rounded endcap. This is indicative of an estimated 3 cm offset of the rotator pole from the geometric centre of the target. This offset was built into the target models. For the following analysis we used 90 time series points (corresponding to 0.1 and 1 msec) and took a 90-point FFT. Even though we know the centre frequency of the cosine-burst used as the incident signal, this signal has a finite bandwidth and the maximum frequency response might be at a slightly different frequency. For our signal analysis, we will consider the FFT bin which contains the largest peak amplitude in the near field (excluding the first or mean level bin). This same bin is then used at the further range. For the inversion data we only consider the first 240 ° of data. This corresponds to one side of the target with some additional angular coverage to adequately sample the flat endcap. One can certainly use 360° or the full 380° of data. However, although there should
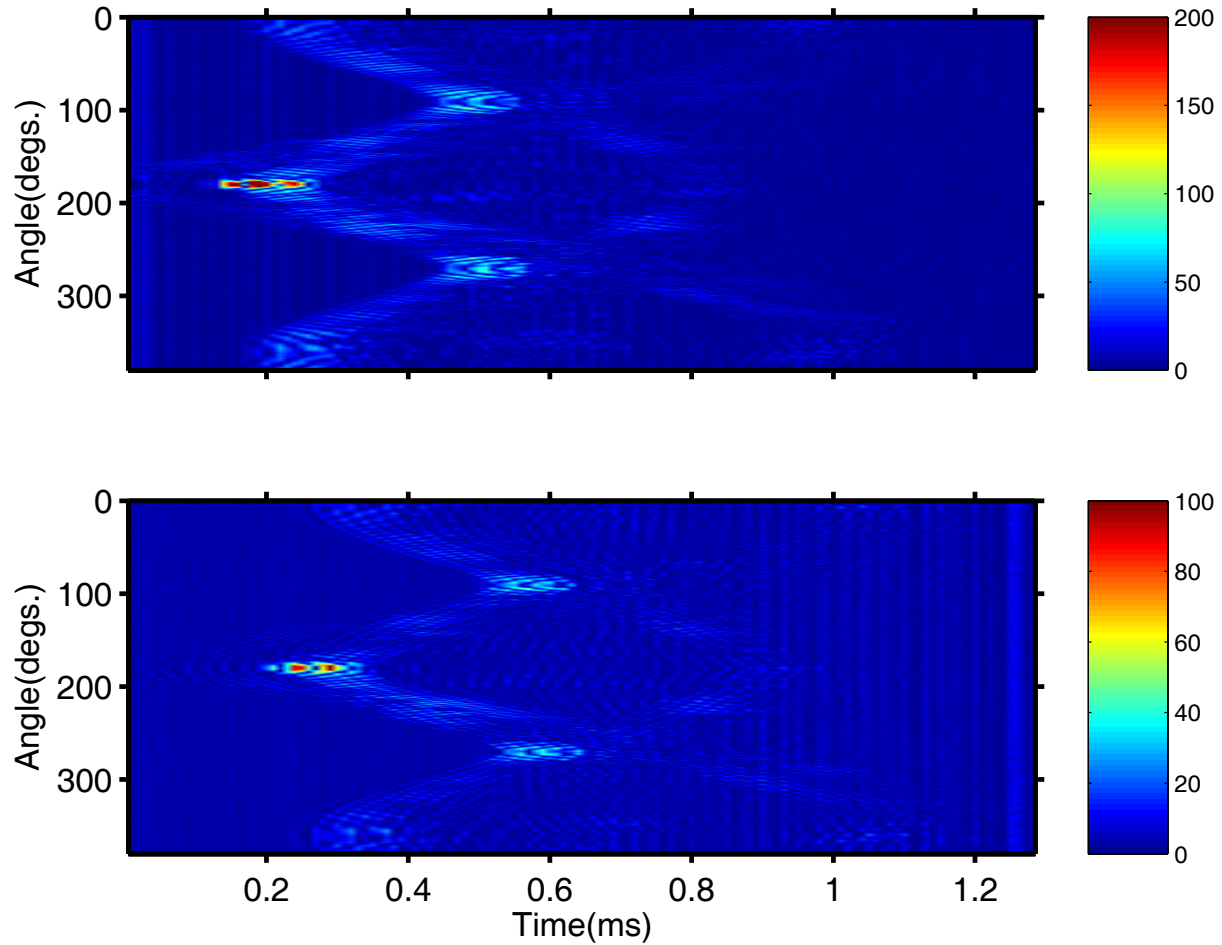
Figure 11: *The time series (absolute value) for the near range (top) and far range (bottom). The extracted backscattered signal is shown as a function of the rotator azimuthal angle. The frequency is 40 kHz.*

be no difference between the scattering from one side of the target to the other, there are some asymmetries. In this case, the set of coefficients which are determined by the inversion will attempt to minimize the model/data error for both sides. It was found that better results were obtained by limiting the data somewhat and considering a single side of the target.

For the model inversion of the near field data, we will consider 2 modified Kirchhoff models, one based upon the simpler structure of Fig. 3a (K1) and one on the more accurate structure of Fig. 3b (K2). It is clear that there are inaccuracies in the modelling for case K2. For example, the slope behind the flat endcap should be in an acoustic shadow for sound directly incident upon this endcap. However, in our case the pressure field from this portion of the target is included in the endcap

scattering computations because the ray/normal condition is still acceptable. Thus, it is not clear whether using a more accurate target model will improve or degrade the model/prediction results. In the sense that we are only attempting to find an "effective" target scattering model, it may make no significant difference. We will also consider the very simple linear array model. In addition, we show the resultant model predictions when we use the standard Kirchhoff approximation with the K2 target model.

As discussed in the theory, there are matrices (S_{jk} in Eq.(6)) which relate the source/receiver angular positions to the point sources, or ring of point sources for the modified Kirchhoff method. These matrices (absolute values) are shown in Fig. 12 for the linear array method, and the modified Kirchhoff methods (K1 and K2). The angle index refers to the measurement angle (for the fixed source and receiver ranges) and the "source index" refers to the unknown coefficients for the point source or rings of point sources. The absolute levels are not important as the Kirchhoff matrices are scaled by the local value of the radius and the arclength between points. It can be seen that the Kirchhoff matrices have a more complicated structure than the matrix for the linear array, although all the matrices are similar in the sense that the largest absolute values correspond to the 2 ends of the target. The singular values of these matrices are important in understanding the stability or robustness of the inversion process. The singular values for the three matrices are shown in Fig. 13 for a frequency of 40 kHz. The distribution of the values for other frequencies is similar although there are fewer significant values at lower frequencies. In our computations, we set a threshold for the singular values in the MATLAB routine for inverting a matrix. This is crucial in the inversion. If the least square inversion is performed with no thresholds, the predicted results are poor. The curves of Fig. 13 give an indication of thresholds to consider. In particular, for the results we present, we used the values of 1.0 for the linear array and 0.001 for the 2 Kirchhoff methods.

In Figs.14-21 a comparison between data and inversion predictions are shown for a variety of frequencies. The first column in Figs. 14-21 show the experimental measurements (blue) and either the predicted or fit (red) values of the near field. The second column shows the measured (blue) and the predicted (red) for the far measurements. The values are scaled by the maximum absolute value of the near field data. Thus, the absolute levels are not shown, but the relative change in the levels from near field to far filed are indicated. We consider 4 methods. The first is that we simply specify the Kirchhoff coefficients as -2 and predict the measurements. The model is scaled so that its norm across angle agrees with the measured field. The near field scaling is used for the far field prediction (i.e., it is not an independent scaling for the far field). The frequencies are 15,20,25,30,35,and 40 kHz, and the results of simply performing this scaled forward modelling are shown in Figs.14 and 15.

Simply modelling the target with the Kirchhoff approximation (and using one simple
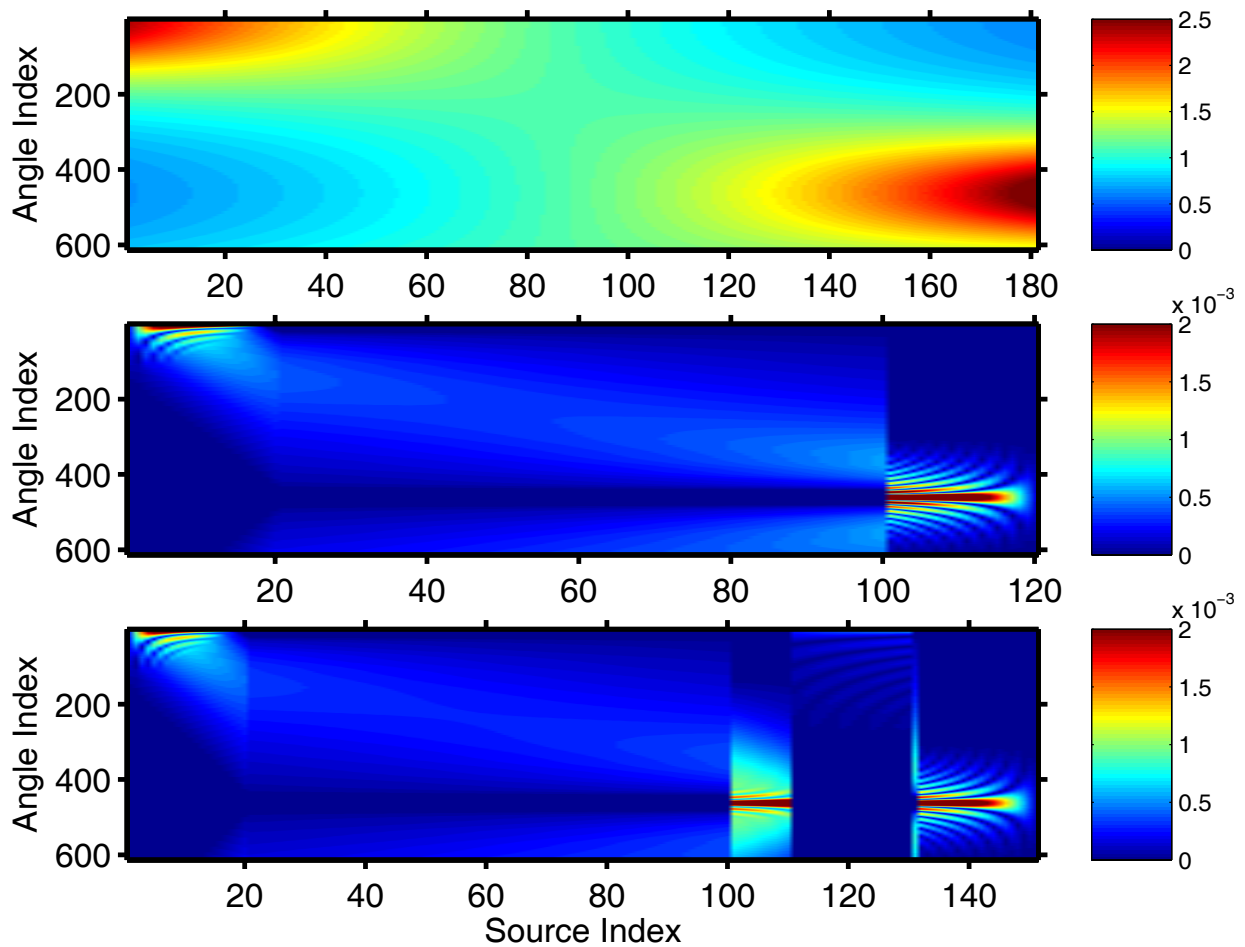
Figure 12: *The matrices used for the inversion process for: (top) linear array (middle) simple Kirchhoff method (bottom) more complicated Kirchhoff method. These are shown for the frequency of 40 kHz.*
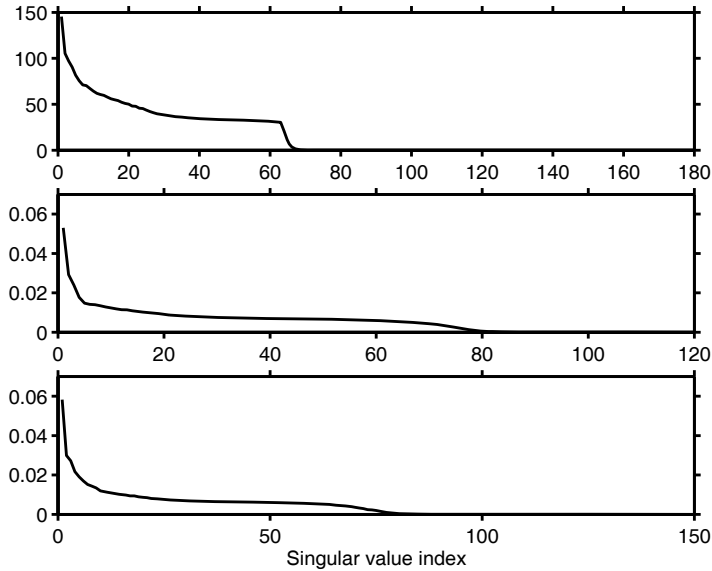
Figure 13: *The singular value distribution for the three matrices at 40 kHz*

scaling) worked rather well. The broadside levels are in good agreement. The end-cap value is quite good, particularly for 15,25, and 40 kHz and not so good at the other frequencies. Some of the other features in the experimental curves seem to be modelled in a "smoothed" fashion. However, much of the detailed target strength structure is not well modelled.

The next 2 figures, Figs. 16 and 17 show the result of using a line array of point sources. The complex amplitudes of these sources are determined from the near field values. Thus, in the first column of these figures, the red curve is the resulting least squares "fit". As can be seen, the predicted levels are in good agreement with the measured results for the broadside and endcap directions (with the exception of 20 Khz, where the measured far endcap level seems anomalously low). In addition, the prediction also captures much of the detailed structure.

For the results of Figs.18-21, we invert for Kirchhoff coefficients where we have used 2 models for the target, a simplified model (Fig.3a) and a more accurate one (Fig.3b). This second model was the same one which was used in the forward Kirchhoff modelling results of Figs. 14 and 15. There is not much difference between the 2 sets of Kirchhoff inversion results. The predictions are excellent. Much of the detailed target scattering structure is very accurately predicted. The one problem for both these methods was the 40-kHz endcap level which was underpredicted.

Figure 14: *The near and far scattering measurements for the peak frequency bin of the near field. The first column is the near measurements (blue) and predictions (red) for 15,20, and 25 kHz. The second column is the same but for further range. For these computations, the Kirchhoff coefficients have been set to a constant. The values have been scaled by the maximum absolute value of the near field data for each frequency.*

Figure 15: *The near and far scattering measurements for the peak frequency bin of the near field. The first column is the near measurements (blue) and predictions (red) for 30,35, and 40 kHz. The second column is the same but for further range. For these computations, the Kirchhoff coefficients have been set to a constant. The values have been scaled by the maximum absolute value of the near field data for each frequency.*

Figure 16: *The near and far scattering measurements for the peak frequency bin of the near field. The first column is the near measurements (blue) and fit curve (red) for 15,20, and 25 kHz. The second column is the same but for further range with predictions in red. For these computations, a linear array of point sources was used. The values have been scaled by the maximum absolute value of the near field data for each frequency.*
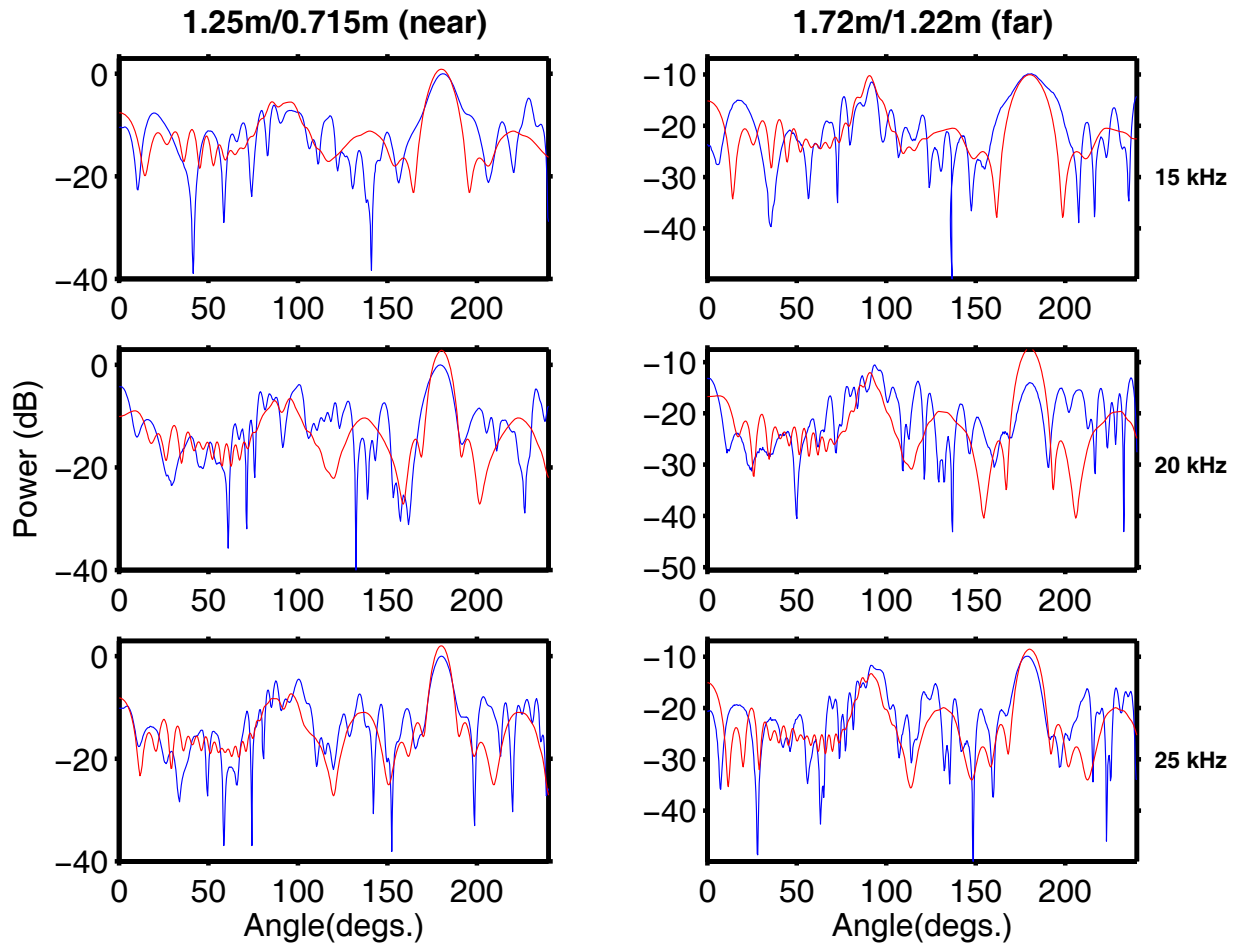
Figure 17: *The near and far scattering measurements for the peak frequency bin of the near field. The first column is the near measurements (blue) and fit curve (red) for 30,35, and 40 kHz. The second column is the same but for further range with predictions in red. For these computations, a linear array of point sources was used. The values have been scaled by the maximum absolute value of the near field data for each frequency.*
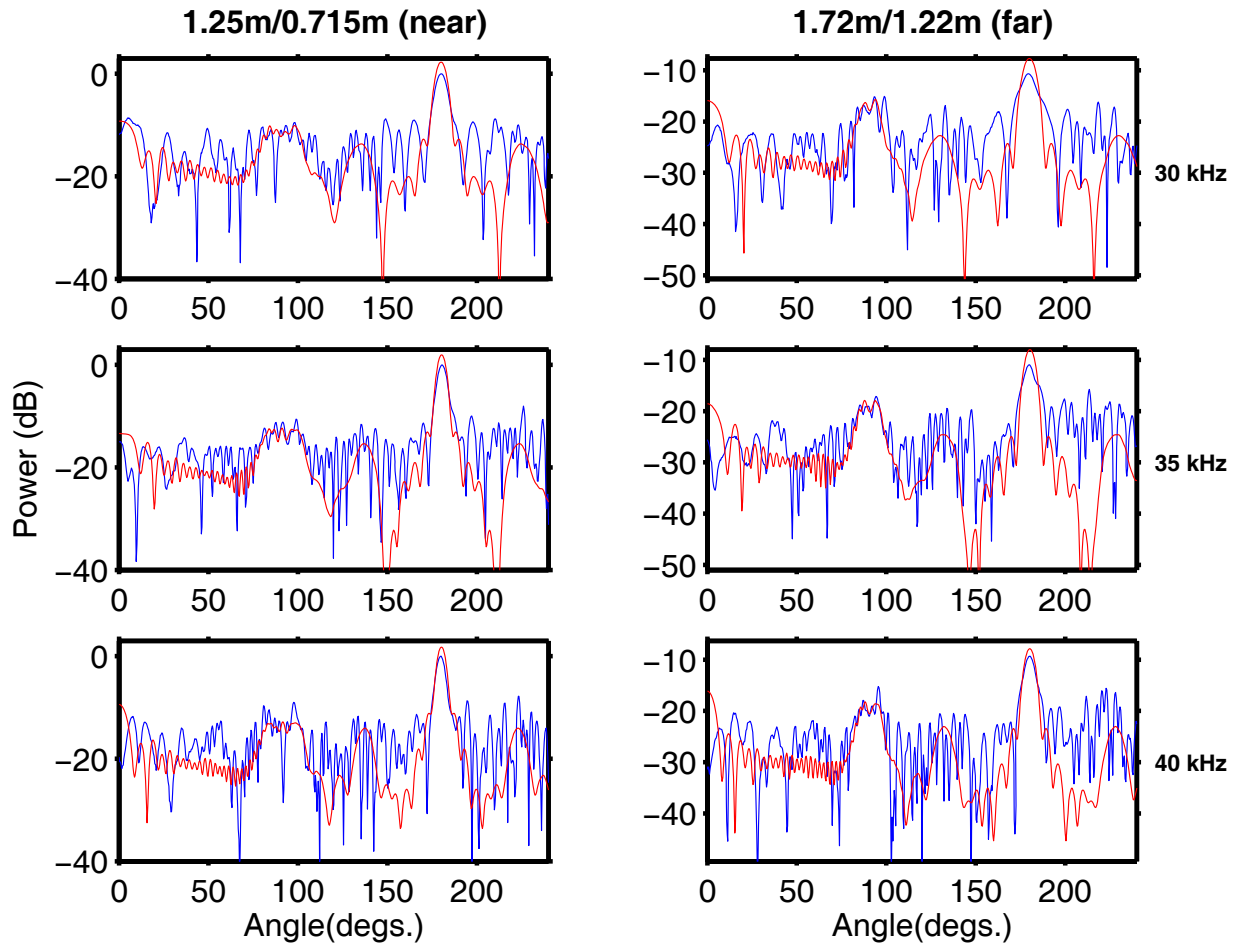
Figure 18: *The near and far scattering measurements for the peak frequency bin of the near field. The first column is the near measurements (blue) and fit curve (red) for 15,20, and 25 kHz. The second column is the same but for further range with predictions in red. For these computations, a simple target model was used as the basis for determining the Kirchhoff coefficients. The values have been scaled by the maximum absolute value of the near field data for each frequency.*
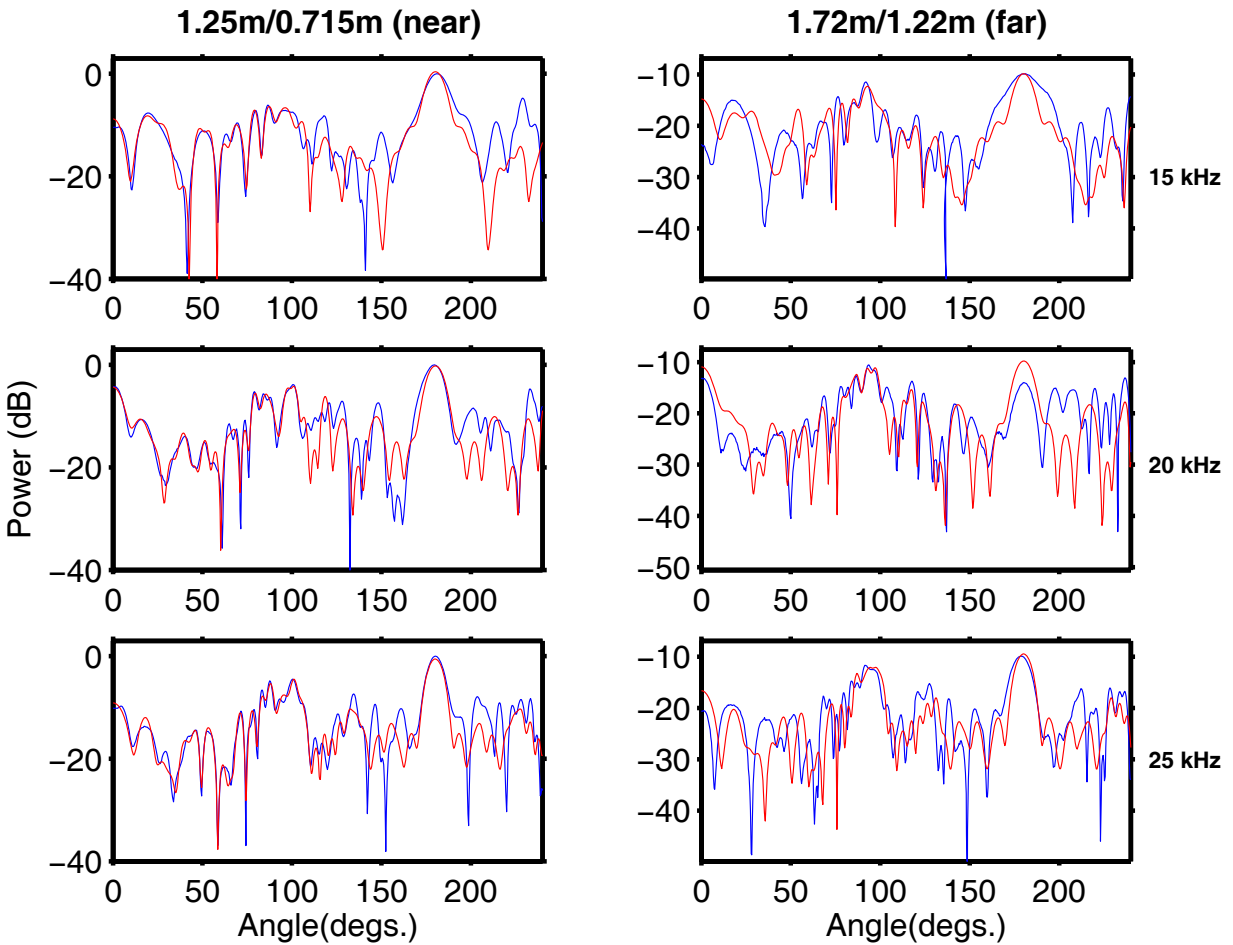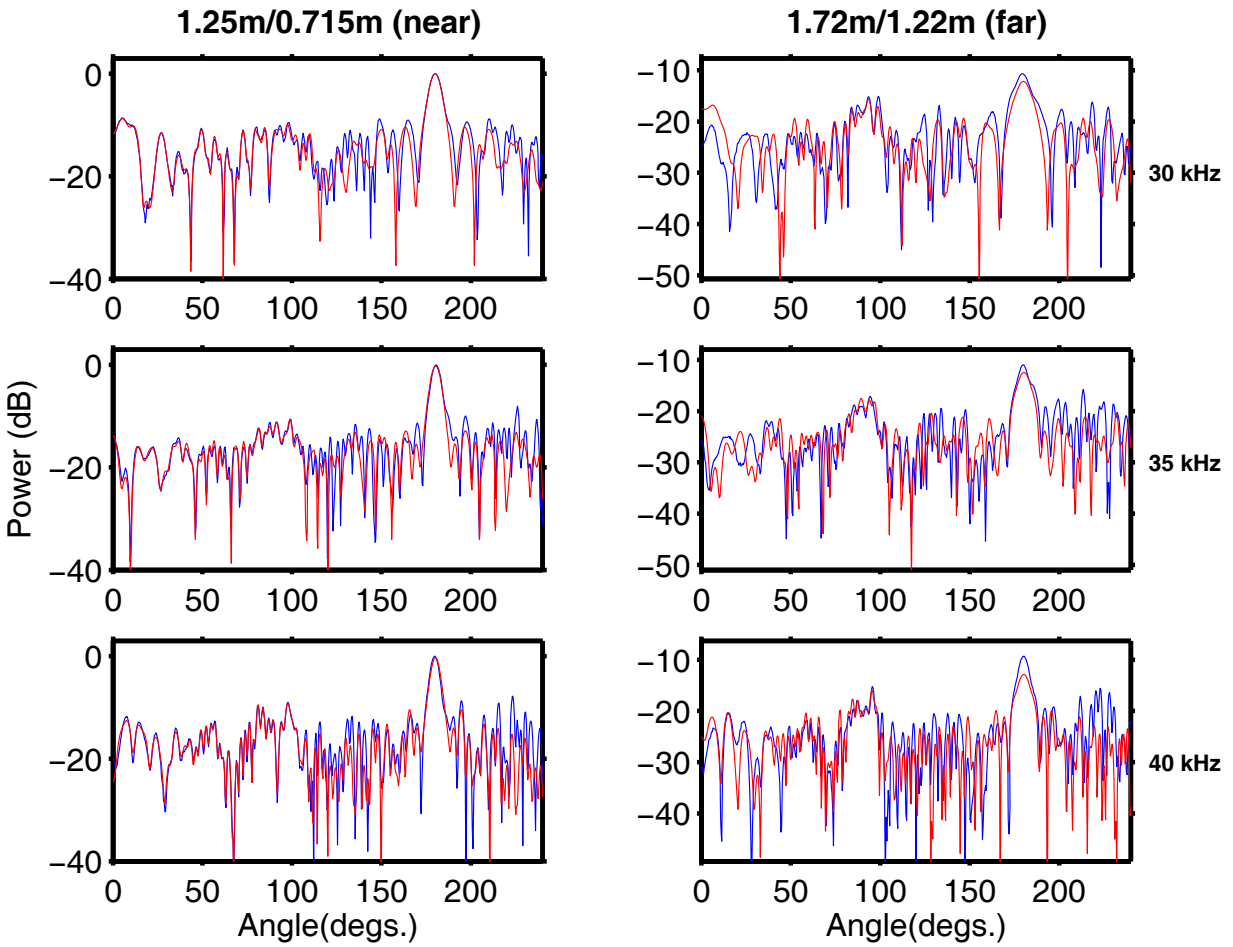
Figure 19: *The near and far scattering measurements for the peak frequency bin of the near field. The first column is the near measurements (blue) and fit curve (red) for 30,35, and 40 kHz. The second column is the same but for further range with predictions in red. For these computations, a simple target model was used as the basis for determining the Kirchhoff coefficients. The values have been scaled by the maximum absolute value of the near field data for each frequency.*
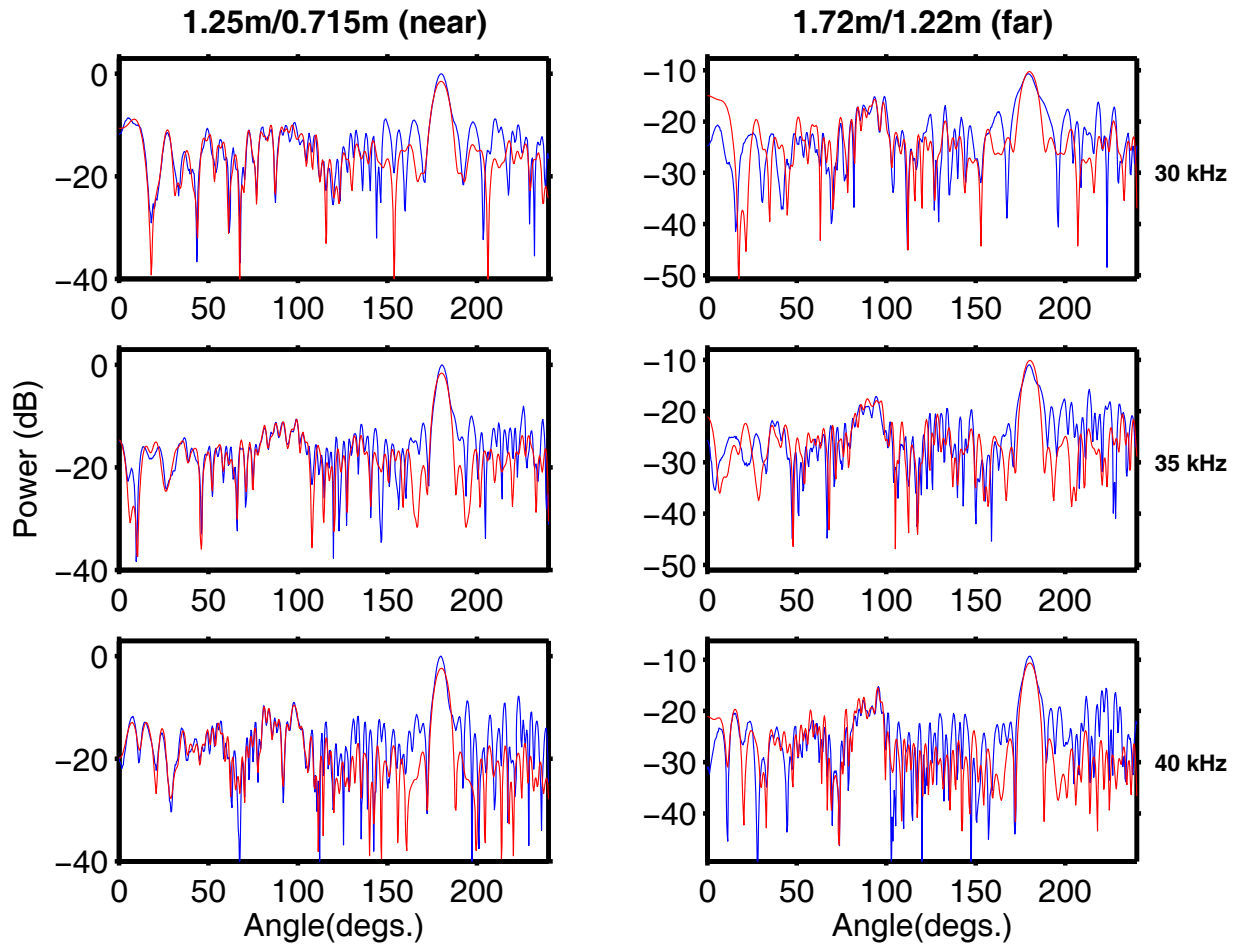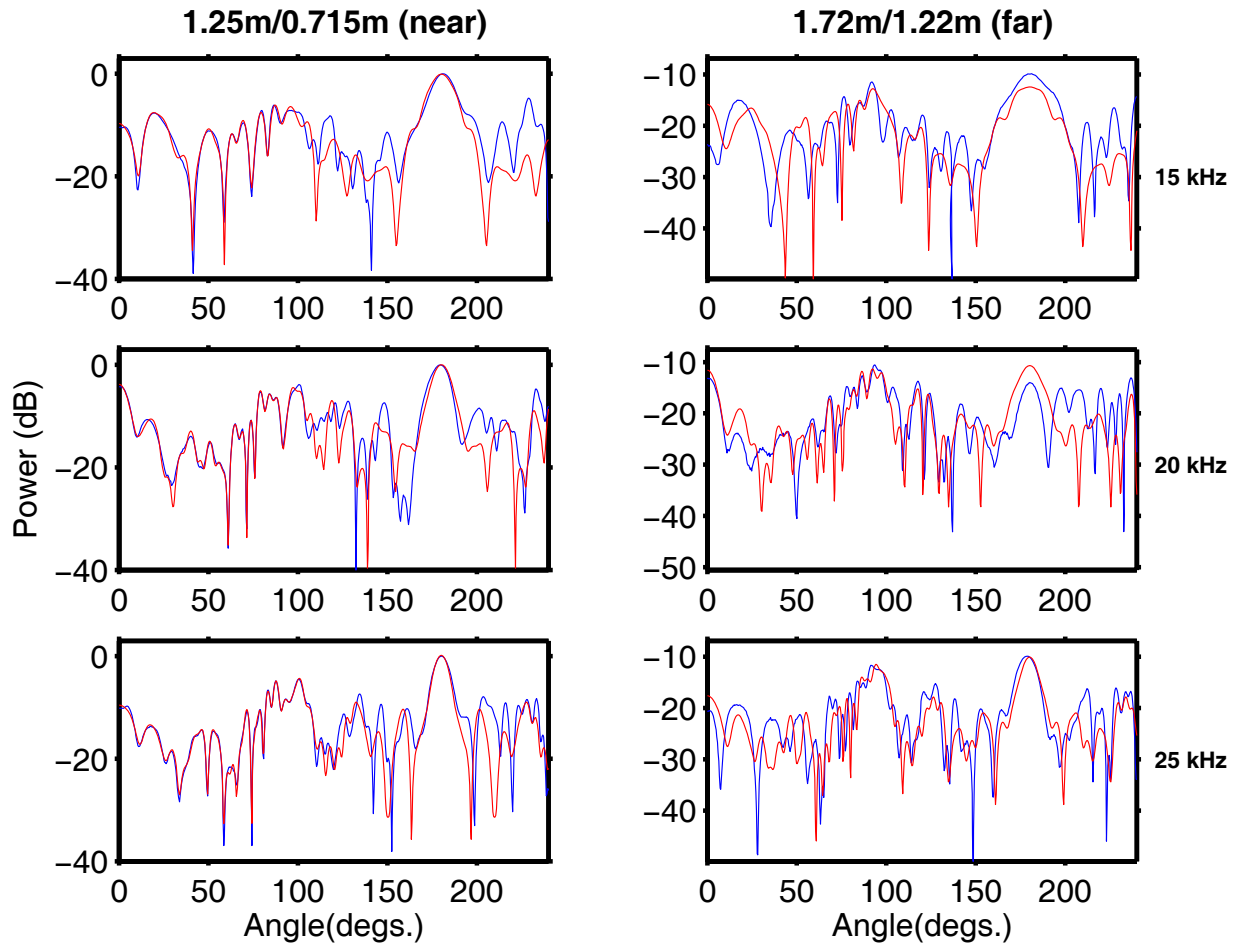
Figure 20: *The near and far scattering measurements for the peak frequency bin of the near field. The first column is the near measurements (blue) and fit curve (red) for 15,20, and 25 kHz. The second column is the same but for further range with predictions in red. For these computations, a more complicated target model was used as the basis for determining the Kirchhoff coefficients. The values have been scaled by the maximum absolute value of the near field data for each frequency.*
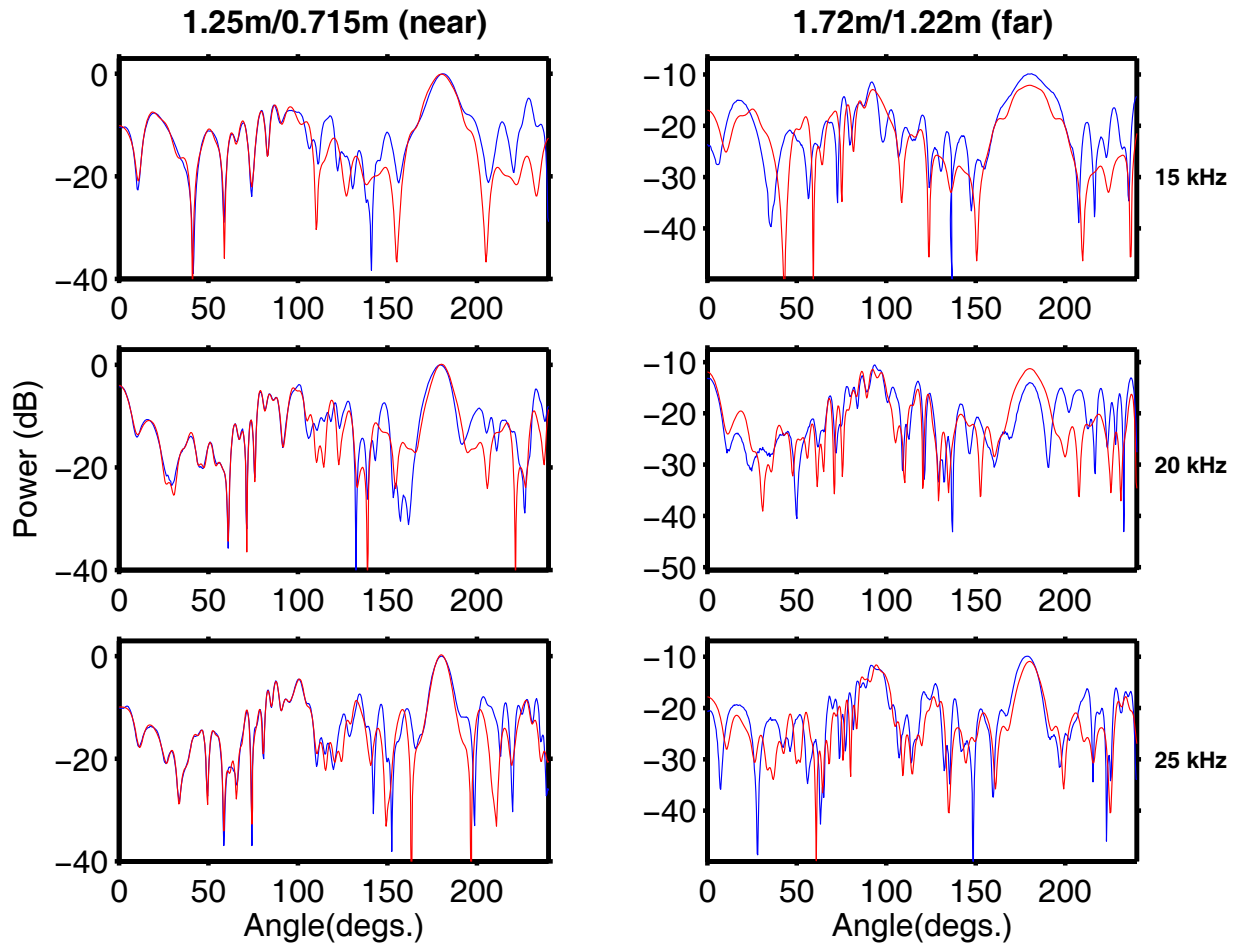
Figure 21: *The near and far scattering measurements for the peak frequency bin of the near field. The first column is the near measurements (blue) and fit curve (red) for 30,35, and 40 kHz. The second column is the same but for further range with predictions in red. For these computations, a more complicated target model was used as the basis for determining the Kirchhoff coefficients. The values have been scaled by the maximum absolute value of the near field data for each frequency.*
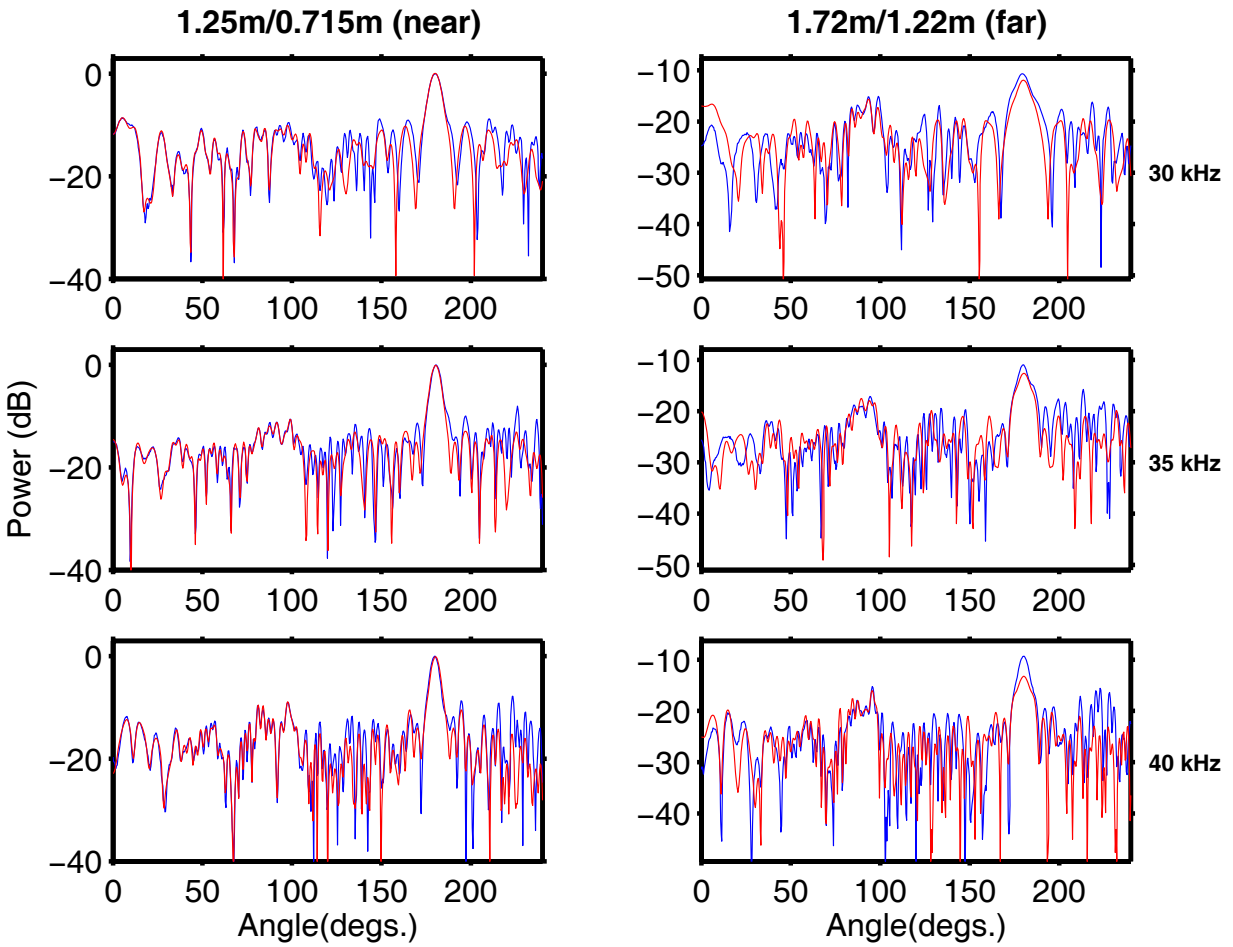
4 SUMMARY

The Kirchhoff method was able predict scattering strengths as a function of aspect angle which were fairly accurate for the broadside and endcap directions. It also correctly predicted some of the other scattering features. However, many of the details of the scattering strength as a function of target aspect were not accurately modelled for the experimental data. For both the numerical and experimental data, very good target strength predictions were obtained using a linear array model. This method accurately predicted the broadside and endcap levels and also captured much of the detailed structure. The Kirchhoff-based inversion method seemed to predict some of the fine detail in the scattering strength curves a little better than the simple linear array approach (although, they underpredicted the 40-kHz endcap level). However, the simpler linear array approach seemed sufficiently accurate for the experimental cases considered. Overall, these inversion approaches certainly seem promising for the prediction of target scattering levels at a specified range from the measurements made at a shorter range. They proved to be sufficiently robust to work with rather noisy experimental data with a complicated target shape.

References

[1] M. Trevorrow, J. Sildam, and L. Gilroy, "Measuremnet and modelling of the acoustic targte strength of a lightweight torpedo", DRDC Atlantic TM 2005-239.

[2] M.C. Junger and D. Feit, *Sound, Structures, and their Interaction*, Acoustical Society of America, 1993

[3] D.M.F. Chapman, "Sonar Target Strength: Theoretical Considerations", DREA Note UA/91/1 (Informal Report), 1991.

[4] J. Nye, "A simple method of spherical near-field scanning to measure the far fields of antennas or passive scatterers", IEEE Transactions on Antennas and Propagation, **51**, pp. 2091–2098, 2003.

[5] S.F. Wu, "Hybrid near-field acoustic holography", J. Acoust.Soc. Am., **115**, pp. 207–217 (2004).

[6] E.G. Williams, "Imaging the sources on a cylindrical shell from far-field pressure measured on a semicircle", J. Acoust. Soc. Am., **99**, pp.2022–2032 (1996).

[7] G.V. Borgiotti and E.M. Rosen, "The determination of the far field of an acoustic radiator from sparse measurement samples in the near field", J. Acoust. Soc. Am., **92**, pp.807–818 (1992).

[8] S.J. Norton and M. Linzer, "Ultrasonic reflectivity imaging in three dimensions: exact inverse scattering solution for plane, cylindrical and spherical apertures", IEEE Transactions on Biomedical Engineering, Vol. BME-28, pp. 202–220 (1981).

[9] B.G. Ferguson and R.J. Wyber, "Application of acoustic reflection tomography to sonar imaging", J. Acoust. Soc. Am., **117**, pp. 2915–2928 (2005).

[10] J. Fawcett, "Finite element modelling of three-dimensional scattering from azimuthally-symmetric elastic shells", SACLANTCEN Report SR-273, 1998.

Distribution List

Internal Distribution

David Hopkin,
Underwater Force Protection Group,
9 Grove St.,
Dartmouth, Nova Scotia, B2Y 3Z7

John Fawcett,
Underwater Force Protection Group,
9 Grove St.,
Dartmouth, Nova Scotia, B2Y 3Z7

Mark Trevorrow,
Torpedo Defence Group,
9 Grove St.,
Dartmouth, Nova Scotia, B2Y 3Z7

Juri Sildam,
Torpedo Defence Group,
9 Grove St.,
Dartmouth,Nova Scotia, B2Y 3Z7

Anna Crawford,
Underwater Force Protection Group,
9 Grove St.,
Dartmouth, Nova Scotia, B2Y 3Z7

Layton Gilroy,
Underwater Signatures Group,
9 Grove St.,
Dartmouth, Nova Scotia, B2Y 3Z7

Library (5)

External Distribution

NDHQ/DRDKIM

This page intentionally left blank.

DOCUMENT CONTROL DATA

(Security classification of title, body of abstract and indexing annotation must be entered when document is classified)

1. ORIGINATOR (the name and address of the organization preparing the document. Organizations for whom the document was prepared, e.g. Centre sponsoring a contractor's report, or tasking agency, are entered in section 8.) Defence R&D Canada – Atlantic P.O. Box 1012, Dartmouth, Nova Scotia, Canada B2Y 3Z7	2. SECURITY CLASSIFICATION (overall security classification of the document including special warning terms if applicable). UNCLASSIFIED

3. TITLE (the complete document title as indicated on the title page. Its classification should be indicated by the appropriate abbreviation (S,C,R or U) in parentheses after the title).

Numerical and experimental investigations of transformations of near-field to far-field scattering measurements

4. AUTHORS (last name, first name, middle initial)

Fawcett, John A. ;   Sildam, J. ;   Trevorrow, M.

5. DATE OF PUBLICATION (month and year of publication of document) July 2006	6a. NO. OF PAGES (total containing information. Include Annexes, Appendices, etc). 46	6b. NO. OF REFS (total cited in document) 10

7. DESCRIPTIVE NOTES (the category of the document, e.g. technical report, technical note or memorandum. If appropriate, enter the type of report, e.g. interim, progress, summary, annual or final. Give the inclusive dates when a specific reporting period is covered).

Technical Memorandum

8. SPONSORING ACTIVITY (the name of the department project office or laboratory sponsoring the research and development. Include address).

Defence R&D Canada – Atlantic
P.O. Box 1012, Dartmouth, Nova Scotia, Canada B2Y 3Z7

9a. PROJECT NO. (the applicable research and development project number under which the document was written. Specify whether project). 11CY04	9b. GRANT OR CONTRACT NO. (if appropriate, the applicable number under which the document was written).

10a. ORIGINATOR'S DOCUMENT NUMBER (the official document number by which the document is identified by the originating activity. This number must be unique.) DRDC Atlantic TM 2006-082	10b. OTHER DOCUMENT NOs. (Any other numbers which may be assigned this document either by the originator or by the sponsor.)

11. DOCUMENT AVAILABILITY (any limitations on further dissemination of the document, other than those imposed by security classification)

(X) Unlimited distribution
(   ) Defence departments and defence contractors; further distribution only as approved
(   ) Defence departments and Canadian defence contractors; further distribution only as approved
(   ) Government departments and agencies; further distribution only as approved
(   ) Defence departments; further distribution only as approved
(   ) Other (please specify):

12. DOCUMENT ANNOUNCEMENT (any limitation to the bibliographic announcement of this document. This will normally correspond to the Document Availability (11). However, where further distribution beyond the audience specified in (11) is possible, a wider announcement audience may be selected).

13. ABSTRACT (a brief and factual summary of the document. It may also appear elsewhere in the body of the document itself. It is highly desirable that the abstract of classified documents be unclassified. Each paragraph of the abstract shall begin with an indication of the security classification of the information in the paragraph (unless the document itself is unclassified) represented as (S), (C), (R), or (U). It is not necessary to include here abstracts in both official languages unless the text is bilingual).

Measurements of monostatic target strength are often made in the near field of the target. This memorandum investigates some model-based inversion techniques which can be used to predict far-field monostatic target strengths as a function of aspect angle from the near field measurements. Simulated and experimental data are used to illustrate the accuracy of the proposed methods.

14. KEYWORDS, DESCRIPTORS or IDENTIFIERS (technically meaningful terms or short phrases that characterize a document and could be helpful in cataloguing the document. They should be selected so that no security classification is required. Identifiers, such as equipment model designation, trade name, military project code name, geographic location may also be included. If possible keywords should be selected from a published thesaurus. e.g. Thesaurus of Engineering and Scientific Terms (TEST) and that thesaurus-identified. If it not possible to select indexing terms which are Unclassified, the classification of each should be indicated as with the title).

near field, far field, target strength

This page intentionally left blank.

Defence R&D Canada

Canada's leader in defence
and National Security
Science and Technology

R & D pour la défense Canada

Chef de file au Canada en matière
de science et de technologie pour
la défense et la sécurité nationale

DEFENCE **R&D** DÉFENSE

www.drdc-rddc.gc.ca